

The prevalence of FR I radio quasars

Ian Heywood, Katherine M. Blundell and Steve Rawlings

University of Oxford Astrophysics, Keble Road, Oxford, OX1 3RH, UK

Accepted 2007 month 00. Received 2007 month 00

ABSTRACT

We present deep, multi-VLA-configuration radio images for a set of 18 quasars, having redshifts between 0.36 and 2.5, from the 7C quasar survey. Approximately one quarter of these quasars have FR I-type twin-jet structures and the remainder are a broad range of wide angle tail, fat double, classical double, core-jet and hybrid sources. These images demonstrate that FR I quasars are prevalent in the universe, rather than non-existent as had been suggested in the literature prior to the serendipitous discovery of the first FR I quasar a few years ago, the optically powerful ‘radio quiet’ quasar E 1821+643.

Some of the FR I quasars have radio luminosities exceeding the traditional FR I / FR II break luminosity, however we find no evidence for FR II quasars with luminosities significantly below the break. We consider whether the existence of such high luminosity FR I structures is due to the increasingly inhomogeneous environments in the higher redshift universe.

Key words: galaxies: active – galaxies: evolution – galaxies: jets – quasars: general – radio continuum

1 INTRODUCTION

The morphological classification scheme for extended extragalactic radio sources described by Fanaroff and Riley (1974) divides these objects into two groups: radio structures decreasing in brightness as the distance from the core increases are classed as FR I and sources with bright hotspots at the extremities are labelled FR II. The two types of object have hitherto been observed to be fairly sharply divided by a luminosity value known as the FR I / FR II break, with FR IIs being the more luminous.

Jets from active galactic nuclei generally give rise to structures which fall into both of these categories although the literature contains assertions that optically powerful quasars with FR I type radio structures do not exist (Falcke et al., 1995; Baum et al., 1995). The general view was that quasars either had luminous FR II structures with hotspots or one sided core-jet structure (radio-loud quasars), or they did not have any significant radio emission other than unresolved cores (radio-quiet quasars). However, these claims were based purely on the absence of FR I quasars from the bright 3C survey together with their absence from limited snapshot (i.e. few minute) radio images in the case of optically selected quasars. The inadequacy and insufficiency of short snapshot images only sensitive to small spatial scales were critiqued by Blundell (2005).

In general, radio observations of quasars to date have consisted of a short ‘snapshot’ observation using the VLA

in the extended A- or B-array configurations (e.g. Miller et al., 1990; Miller et al., 1993; Kellermann et al., 1994; Hooper et al., 1996; Kukula et al., 1998; Goldschmidt et al., 1999; White et al., 2000). Observations of this type would be inadequate for detecting FR I structures for two reasons. First, as the name would imply the integration time of a snapshot observation is generally short (≤ 5 minutes) which compromises the sensitivity and ability to perform high-fidelity deconvolution. Second, the extended configurations of the VLA will resolve out the extended structures with low intensity gradients, features which are characteristic of FR I sources. Thus it is at least plausible that observations to date have not detected smooth, faint 100-kpc-scale FR I structures with quasars simply because the observations have been inadequate.

It is also noteworthy that the luminosity of every previously identified FR I source is below or very close to the FR I/FR II break luminosity, which at 178 MHz is $\sim 10^{25.5} \text{ W Hz}^{-1} \text{ sr}^{-1}$ (Fanaroff & Riley, 1974). This explains the lack of FR I structures associated with quasars found so far as the FR I/FR II break luminosity falls below the flux limit at the rather low redshift of 0.4, for some of the current deepest low-frequency selected complete samples (Rawlings et al., 1998; Blundell, Rawlings & Willott, 1999).

This leads on to the final consideration for the apparent lack of FR I quasars. The rarity of quasars implies that large volumes of space must be searched in order to observe one or more FR I sources. Generally quasars are found at

redshifts greater than 0.4, and as more distant quasars are observed the feasibility of detecting a low-luminosity FR I source decreases for a radio flux-limited survey.

Given that jets of both FRI and FRII morphologies are common for many types of active galaxy, coupled with the above observational considerations, it is plausible that the lack of FRI-type quasars is not due to the fact that they do not exist but because the existing observations and radio surveys are simply not detecting them. In fact the first *deep* image of the so-called radio quiet, optically powerful quasar E1821+643 serendipitously revealed a 300 kpc FRI jet structure (Blundell & Rawlings, 2001).

With this discovery and the limitations of previous observations firmly in mind VLA observations of 18 quasars selected from the 7C quasar survey (Riley et al., 1999) were scheduled. The objects selected were FRI candidates from the 7C quasar survey and details of the selection criteria and the observations can be found in Section 2. In Section 3 we present combined multi-VLA-configuration radio images and flux density measurements of the 18-object sample. Section 4 contains morphological discussions on a per-source basis, as well as redshift-dependent considerations both for our sample and for FRI quasars in general. Concluding remarks are presented in Section 5.

Throughout this paper the $H_0 = 70 \text{ km s}^{-1} \text{ Mpc}^{-1}$, $\Omega_M = 0.3$ and $\Omega_\Lambda = 0.7$ cosmology is used.

2 SAMPLE SELECTION, OBSERVATIONS AND DATA REDUCTION

The starting point for the sample selection was the 7C quasar survey (Riley et al., 1999). This ‘filtered sample’ of quasars was chosen from a complete sample selected to be brighter than 100 mJy at the low radio frequency of 151 MHz, and optical colour filters were applied to favour the detection of quasars.

Beginning with the Riley et al. sample, we took the bona fide quasars (confirmed via unpublished optical spectra; Rawlings, priv. comm.) and plotted their radio flux density measurements from the FIRST survey (Becker et al., 1995) against those of the NVSS survey (Condon et al., 1998), as can be seen in Figure 1. The FIRST and NVSS surveys were carried out with the VLA in its B- and D-array configurations respectively. Higher flux density values in D-array observations when compared to those of B-array at the same frequency are an indicator that there is undetected extended structure.

In Figure 1 we see many objects with clear indications of extended structure. Given the finite amount of observing time available, we could neither observe all objects in the sample nor all objects with evidence of extended structure. The sample we chose to observe is therefore in no sense complete but we believe it to be representative of the 7C quasar survey. The 18 quasars we observed are listed in Table 1

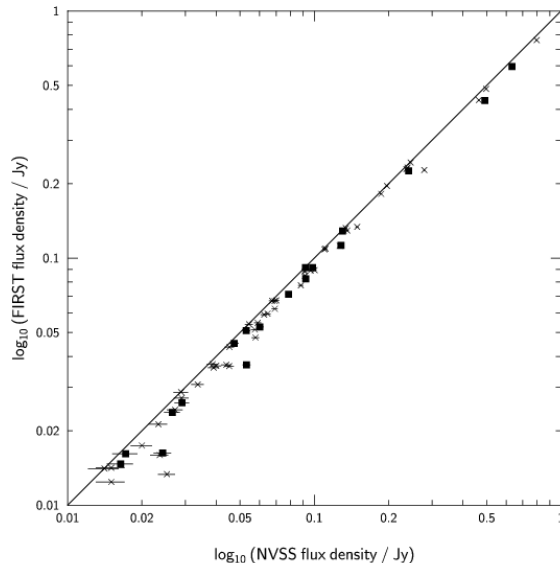


Figure 1. The FIRST against NVSS radio flux density measurements for the confirmed radio quasars from the 7C quasar sample (Riley et al., 1999). Objects selected for our radio observations are represented by the filled square symbols. Errors for both the FIRST and NVSS flux densities are plotted. The NVSS errors are generally too small to be seen in the upper half of the plot. Errors in the FIRST flux density measurements are invisible throughout, although it is noteworthy that these are only the quoted RMS values and do not include “systematic” errors (e.g. from missing flux).

which also lists their spectroscopically measured redshifts.* Figure 2 shows the selected quasars in the P - z plane.

In an attempt to overcome the problems faced by previous radio observations of quasars the data obtained for the sample involved reasonably long integration times with all four configurations of the VLA. We observed using the A-, B-, C- and D-arrays at 1.4 GHz and then combined the data facilitating the sampling of the maximum possible range of Fourier components, boosting the signal to noise ratio of the final images and also favouring optimal deconvolution.

A summary of the observations can be found in Table 2. The primary and secondary calibrator sources were 1331+305 (3C 286) and 1033+412 respectively. A single ~ 2 minute observation of the primary flux calibrator 1331+305 was carried out for each array configuration and phase-calibrator 1033+412 was observed for ~ 1 minute intervals, approximately once per hour.

Processing of the data was carried out using standard procedures, including phase self-calibration, in AIPS. The flux density scale was calibrated according to the methods of Baars et al. (1977). Any suspicious or bad visibili-

* The sample of Riley et al. (1999) has almost complete optical spectroscopy providing confirmation (or in a few cases rejection) of the quasar hypothesis via detection of broad lines as well as measurements of redshifts. Spectra were gathered using, variously, the Isaac Newton Telescope (with the Faint Object Spectrograph, FOS-1), The William Herschel Telescope (using ISIS and FOS-2) and the Nordic Optical Telescope (with Low-Dispersion Spectrograph).

Table 1. The sample of 18 quasars from Riley et al’s (1999) quasar sample. This table shows the object names for both the J2000 and B1950 epochs as well as the central pointing coordinates used for the VLA observations in J2000 format, and the redshift of each quasar. The classification abbreviations are as follows: CD – classical double, FD – fat double, TJ – FR I twin jet source, CJ – core-jet source, WAT – wide angle tail (see Section 4.1), X – undetermined .

Source		RA (J2000)	Dec (J2000)	z	Classification
(J2000)	(B1950)				
1009+4655	1006+4710	10 09 40.601	+46 55 23.03	1.010	FD
1018+3542	1015+3557	10 18 10.989	+35 42 39.27	1.226	CJ
1021+4523	1018+4538	10 21 06.048	+45 23 31.64	0.363	FD
1022+3931	1019+3947	10 22 37.459	+39 31 50.03	0.607	CD
1023+3604	1020+3619	10 23 15.762	+36 04 35.41	1.320	TJ
1023+4414	1020+4429	10 23 29.805	+44 14 14.21	0.750	WAT?
1023+4824	1020+4839	10 23 29.794	+48 24 36.99	1.231	CD
1029+3224	1027+3239	10 29 59.132	+32 24 19.42	1.187	CJ
1030+3346	1027+3401	10 30 15.780	+33 46 32.17	1.050	TJ
1030+4309	1027+4324	10 30 21.547	+43 09 07.84	1.112	TJ
1032+4932	1029+4948	10 32 34.851	+49 32 43.52	2.452	CD
1033+4116	1030+4131	10 33 03.705	+41 16 06.09	1.120	X
1037+4650	1034+4705	10 37 15.391	+46 50 14.31	2.150	TJ
1038+3729	1035+3745	10 38 48.131	+37 29 24.48	0.731	FD
1040+4449	1037+4505	10 40 22.792	+44 49 36.75	0.590	TJ
1040+4529	1037+4545	10 40 42.316	+45 29 39.57	1.475	CJ
1054+4541	1051+4557	10 54 32.103	+45 41 52.29	2.500	TJ
1057+4556	1054+4612	10 57 18.453	+45 56 15.16	2.130	CD

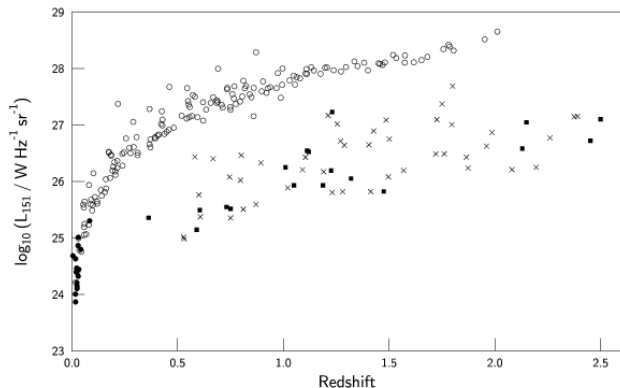


Figure 2. Source luminosity at 151 MHz against redshift for the 3C survey (circles, with known FR I objects represented by the filled markers) and the 7C survey (crosses, with the 18 quasars selected for this paper represented by the filled squares).

Table 2. Summary of the VLA observations.

Array configuration	Observation date	Approximate on-source integration time
A	2004 Sep 18	2×10 minutes
B	2003 Dec 19	2×15 minutes
C	2004 May 10	1×15 minutes
D	2004 Jul 29	2×3 minutes

ties were flagged using the TVFLG task in AIPS. Combining and cross-calibrating data from the different array configurations using IMAGR, CALIB and DBCON was straightforward,

although in certain cases strong confusing sources had to be removed from the more compact configuration data by means of subtraction of a clean component model (IMAGR, CCEDT, UVSUB). The final combined data sets were cleaned and imaged using IMAGR. Flux density measurements were made using TVSTAT, or IMFIT in the case of the unresolved sources given by certain compact array observations.

3 RESULTS

3.1 Radio maps

Figures 3, 4 and 5 show the combined array 1.4 GHz radio images for the 18-quasar sample. Table 3 shows a summary of the final image parameters. The fitted beam describes the half-power dimensions and position angle of a 2D Gaussian fitted to the point spread function for each image. In each case this is used as the restoring beam when mapping. Each image is created with the maximum possible resolution (i.e. equivalent resolution of an A-array observation), except in the cases of 1023+4414 and 1038+3729 where the spatial resolution is degraded in order to highlight the interesting larger scale structures. This process is reflected in the fitted beam sizes listed in Table 3.

For each image the lowest contour has a value of minus $\sqrt{2}$ times 2.5σ , where σ is the rms background noise measured on each image. Following this single negative value, contours begin at 1 and increase in multiples of $\sqrt{2}$ times (σ). The grey scale pixel range runs from 2 times the rms noise to the peak flux density in milli-Janskys per beam. The crosshairs on each map show the central pointing coordinates as listed in Table 1 and are coincident with the optical positions of the quasars. The crosshairs span 1.5 arcseconds.

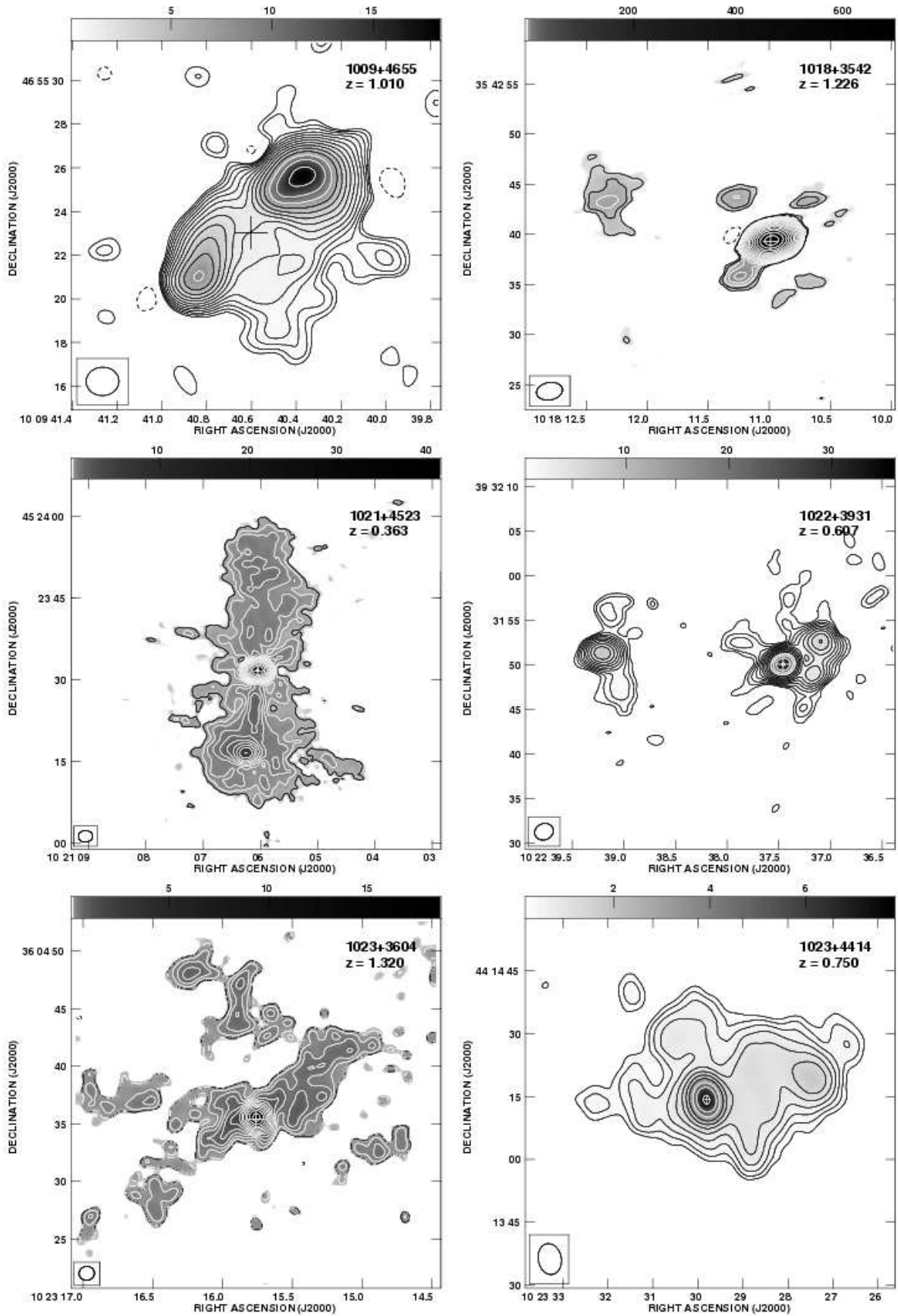


Figure 3. VLA images 1.

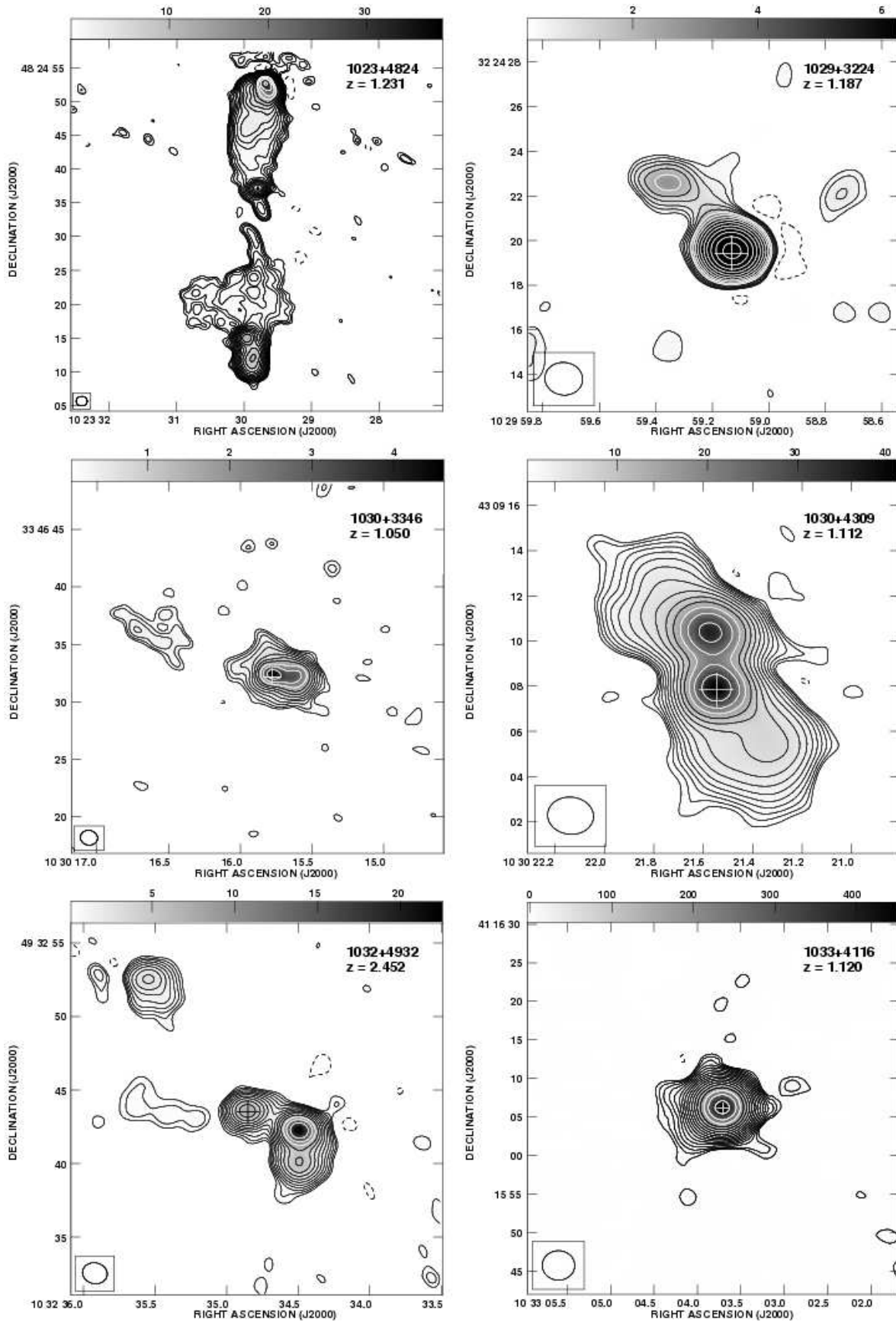


Figure 4. VLA images 2.

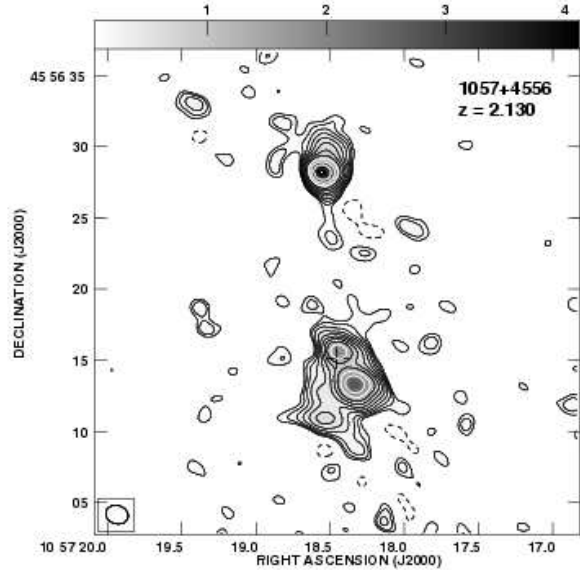
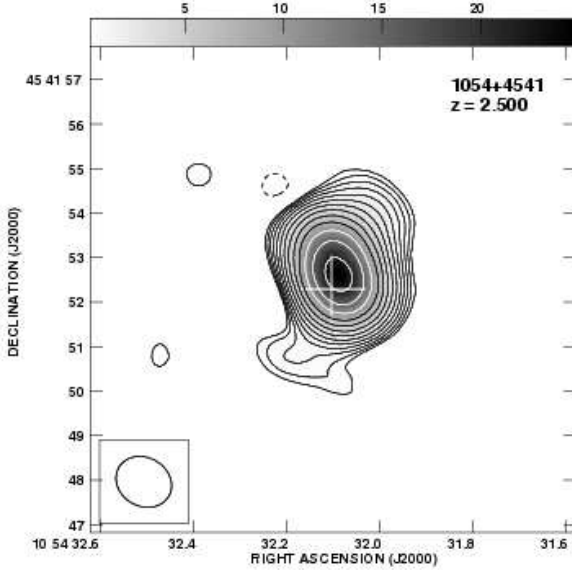
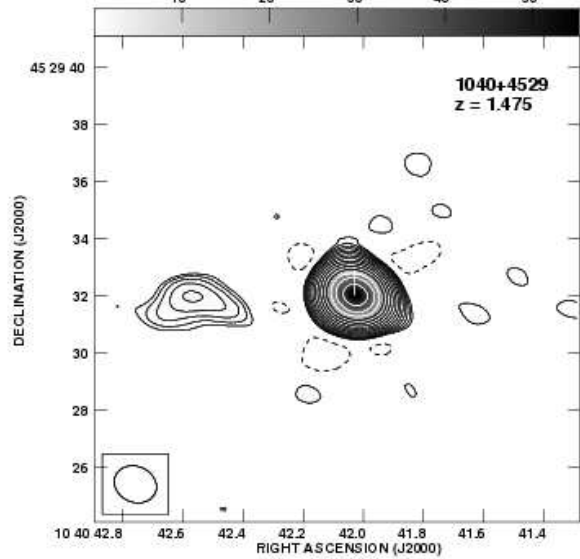
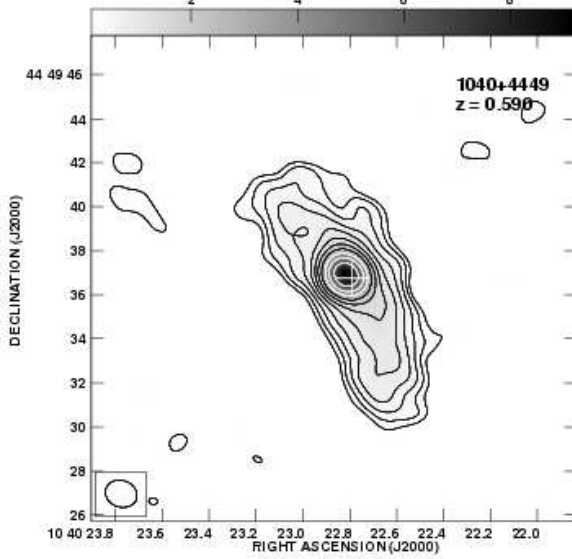
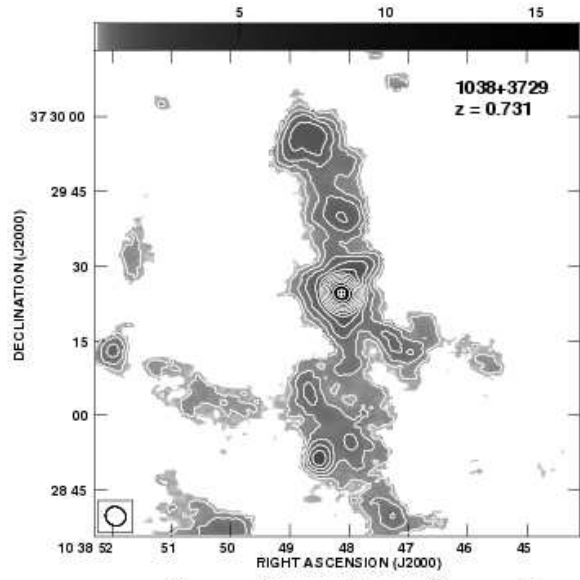
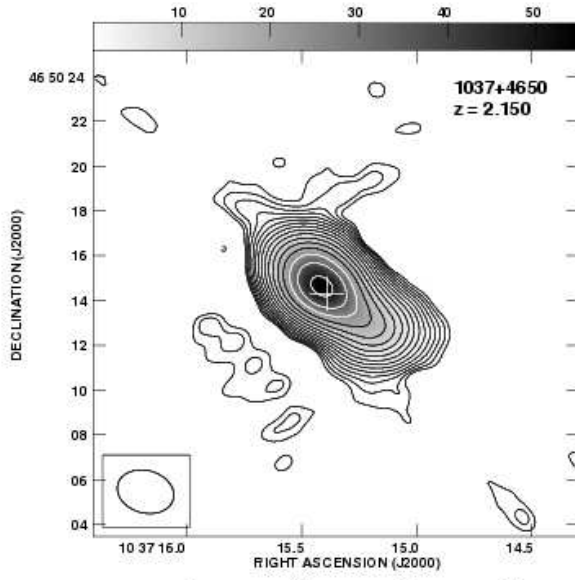


Table 3. Summary of the radio maps presented in Figures 3, 4 and 5. The contour multiplier is 2.5 times the rms background noise in each image and the grey scale pixel range runs from 2 times the rms noise to the peak flux in mJy / beam.

Source	Fitted beam (arcseconds)	PA (degrees)	Contour multiplier mJy / beam	Greyscale range mJy / beam	Transfer function	Core visible in A-array at 1.4 GHz? (Yes/No)
1009+4655	1.50×1.30	-87.12	0.175	0.14 – 18.25	Linear	No
1018+3542	2.60×1.72	-79.83	1.570	1.26 – 694.95	Logarithmic	Yes
1021+4523	2.63×2.14	-87.51	0.313	0.25 – 41.21	Logarithmic	Yes
1022+3931	2.13×1.81	-68.39	0.389	0.31 – 36.09	Linear	Yes
1023+3604	1.34×1.20	-82.12	0.250	0.20 – 18.49	Logarithmic	Yes
1023+4414	7.47×5.50	10.72	0.231	0.19 – 7.83	Linear	Yes
1023+4824	1.62×1.43	87.73	0.142	0.11 – 37.62	Linear	Yes
1029+3224	1.70×1.46	83.31	0.424	0.34 – 6.25	Linear	Yes
1030+3346	1.50×1.27	80.35	0.118	0.09 – 4.59	Linear	Yes
1030+4309	2.04×1.65	85.07	0.350	0.28 – 41.50	Linear	Yes
1032+4932	1.69×1.42	78.28	0.253	0.20 – 22.47	Linear	Yes
1033+4116	4.22×3.82	89.33	1.538	1.23 – 451.00	Linear	Yes
1037+4650	2.56×1.90	74.74	0.276	0.22 – 54.58	Linear	Yes
1038+3729	4.15×3.76	65.43	0.319	0.26 – 16.29	Logarithmic	Yes
1040+4449	1.46×1.21	70.04	0.207	0.14 – 9.23	Linear	Yes
1040+4529	1.51×1.25	66.47	0.340	0.24 – 55.23	Linear	Yes
1054+4541	1.30×1.07	61.00	0.338	0.27 – 24.75	Linear	Yes
1057+4556	1.60×1.28	72.40	0.091	0.07 – 4.11	Linear	Yes

3.2 Radio flux density measurements

Radio flux density measurements for the sample are presented in Table 4 as determined by isolating the source structure in AIPS with a box and executing the TVSTAT verb. The error quoted is determined by the rms noise in the background of the image. The table contains the 1.4 GHz flux densities as measured from the A-, B-, C- and D-array observations. Note that the errors quoted are from map-specific flux density ratios which are accurate to better than one percent. Errors in the absolute flux values, due to the calibration according to the Baars scale, are typically a few percent (Perley, private communication and in prep.) and have not been included here.

The flux densities from the FIRST and NVSS surveys are also presented for comparison. Generally for sources with extended structure the flux-density measurements would be expected to rise as the array becomes more compact and the Fourier plane sampling becomes more favourable for the detection of larger scale structures. This effect can be seen in several of the sources from the sample (1021+4523, 1022+3931, 1023+4414, 1038+3729, 1040+4449, 1054+4541 – see discussion in Section 4.1) and in the cases where no compact hotspots are present this suggests they are of the FRI type. The NVSS survey was conducted with the D-array and the flux-density values measured from these observations are normally in good agreement with the D-array measurements obtained for this study except in the case of variable sources, which we address in Section 4.1 on a source by source basis. Similarly, except where noted in Table 4, the B-array flux-density measurements are in good agreement with the FIRST survey, also made using the VLA in B configuration.

4 DISCUSSION

Whether a source is classified as an FRI or an FR II is determined by the morphology from radio imaging (Fanaroff and Riley, 1974). If the source is edge brightened at the extremities and with compact hotspots then it is generally of the FR II (i.e. classical double) type.

The radio maps presented in Figures 3, 4 and 5 show a variety of different structures. Generally the objects can be classed as either classical double FR II sources or the FRI type twin jet sources, however there are also the more ambiguous structures which could be classified as fat doubles (Owen & Laing, 1989) or hybrid sources (Gopal-Krishna & Wiita, 2002).

A discussion of each quasar follows, including morphological deductions from the radio images and the behaviour of the measured flux density with uv coverage. Certain objects have also been previously observed at 8 GHz using the VLA in B-array. The features visible in these unpublished maps are discussed where relevant. The increased resolution provided by the high frequency observations is useful for identifying compact regions of enhanced surface brightness. Features such as these arising at the extremities of the object are thought to coincide with the shock fronts occurring as the jets collide with the ambient medium forming hotspots. These are generally taken as evidence that the kinetic energy of the jet is still feeding the lobe head. Rounded, edge-brightened lobes which lack compact hotspots are generally a property of a fat double source. Objects are classified as FRI twin jet sources when they exhibit large-scale extended radio structure that is similar to what is seen to arise from the twin-jet radio sources in the nearby Universe.

4.1 Discussion of individual sources

1009+4655: This source shows two bright lobes with extended emission. There is no compact object visible at the central pointing position. Examination of the 8-GHz image

Table 4. Flux density measurements for the sample of 18 7C quasars. Results from all four VLA array configurations are presented together with the values derived from the B-array FIRST survey and the D-array NVSS survey.

Source (J2000)	1.4 GHz Flux Density (mJy)				FIRST	NVSS	Notable flux differences for possible variability
	A-array	B-array	C-array	D-array			
1009+4655	71.5±0.2	69.0±0.9	74.7±0.2	70.0±0.6	70.6	77.3	–
1018+3542	676.6±3.9	650.0±3.0	695.0±1.0	682.0±3.4	594.1	615.2	B/FIRST; D/NVSS
1021+4523	45.4±0.3	88.8±0.1	122.0±0.1	122.3±0.8	98.2	127.2	–
1022+3931	76.9±0.3	82.9±0.1	84.9±0.6	94.8±2.2	79.2	91.2	–
1023+3604	20.6±0.2	22.1±0.2	29.0±0.1	24.0±1.0	25.3	28.4	–
1023+4414	7.7±0.2	7.9±0.1	25.8±0.3	23.8±0.8	12.9	23.6	–
1023+4824	203.6±0.2	211.0±0.1	230.0±0.2	227.7±0.6	224.2	239.5	–
1029+3224	62.4±0.4	63.2±0.9	73.6±0.3	74.3±1.0	89.9	96.3	B/FIRST; D/NVSS
1030+3346	14.5±0.1	14.3±0.1	18.5±0.2	16.7±1.2	14.1	16.4	–
1030+4309	124.0±0.2	120.7±0.4	126.6±0.2	124.4±1.3	125.9	129.9	–
1032+4932	47.1±0.2	39.3±0.1	45.6±0.1	42.0±0.9	44.3	46.8	–
1033+4116	436.8±2.4	458.8±0.7	518.2±0.2	515.8±1.6	432.7	473.2	B/FIRST; D/NVSS
1037+4650	81.5±0.6	80.2±0.2	84.9±0.2	81.5±0.5	89.8	90.2	B/FIRST; D/NVSS
1038+3729	14.7±0.3	31.2±0.3	43.8±0.5	55.0±1.2	29.2	54.3	–
1040+4449	9.2±0.3	15.4±0.1	23.0±0.1	20.8±1.0	14.7	23.0	–
1040+4529	53.6±0.5	50.9±0.2	55.2±0.1	52.7±0.8	51.8	53.4	–
1054+4541	44.6±0.4	47.3±0.2	52.2±0.2	51.5±1.0	49.7	52.3	–
1057+4556	9.1±0.1	9.3±0.1	17.3±0.1	15.9±0.2	15.8	14.9	B/FIRST

reveals that the two peaks present in the 1.4-GHz image are each resolved into elongated jet-like features as seen in some FR Is. These do not appear compact in the high resolution image. The axial ratio means that this object would most likely be classified as a fat double. The diffuse low brightness extensions to the south west of the object may be plumes of emission diverted at right angles to the jet axis.

1018+3542: The flux-density behaviour of this object points to high variability and does not suggest any structure is being resolved out at any stage. This source is by far the brightest object in the sample, at almost 0.7 Jy, and it is likely that the strength of the core is limiting the dynamic range of the image making detection of extended low surface brightness emission difficult. The features which are detected hint at the presence of a highly asymmetric structure, as is consistent with several other objects in this sample (see below). This may be a consequence of relativistic Doppler boosting.

1021+4523: The flux density values for this object increase with decreasing array size suggesting undersampling of smooth extended structure by the extended arrays. This would usually be an indicator of an FRI type object however the southern part of this object appears to contain a compact hot spot with a coherent structure linking it to the core. This unusual object would probably be classified as a fat double, or hybrid source. This object exhibits similarities with hybrid sources such as 0131–367 (Gopal-Krishna & Wiita, 2002) with jets of FRI and FRII characteristics on different sides of the nucleus. It is also noteworthy that the southern hotspot is recessed somewhat from the outer edge of the emission, as seen in some fat doubles (Owen & Laing, 1989).

1022+3931: The central pointing coordinates are coincident with the brightest of the four components visible in the map. The next brightest peak to the north west of the core is most likely a hotspot and this object is probably

a FRII classical double. No emission linking the quasar to the peak visible to the east was found, even by varying the size of the restoring beam. It is likely however that this is emission from a second hotspot.

1023+3604: This source can be classified as a FRI twin jet source even though the extended structure is very close to the noise in the map. The extended emission on each side of the core share a parallel axis even though they are slightly offset from the core. This is characteristic of a single twist in the jets although precession of the jet axis may also be a possibility (c.f. E 1821+643, Blundell & Rawlings, 2001, and 3C294, Erlund et al., 2006).

1023+4414: The spatial resolution of this image was deliberately degraded in order to reveal the extended emission. Higher resolution imaging showed only the core and the peak to the west, resolving out the diffuse envelope surrounding them. The fifth positive contour hints at meandering emission with a comparatively large transverse angular size. While features such as these are indicative of wide angle tail sources, our classification for this object remains inconclusive.

1023+4824: The best example of a classical double FRII structure in the sample, 1023+4824 shows extensive edge brightening, a compact core and hotspots and asymmetrical jets. The southern lobe shows what appears to be a region of extended backflow. Classical doubles with large angular sizes will exhibit variations in flux density with larger baseline arrays, hence our selection criteria will not fully exclude objects such as this one.

1029+3224: This source exhibits a variable core and the flux density values hint at some extended structure being resolved out. Maximum resolution imaging reveals a core-jet structure with a partially resolved north eastern extension linked to the core.

1030+3346: Figure 4 shows the maximum resolution map for 1030+3346 showing FRI type emission coming from

the west of the core. The diffuse feature to the east of the object is probably associated with the quasar. In a similar way to the maximum resolution image of 1029+3224 the emission to the east appears as a secondary low brightness peak connected to the core in both the B-array data associated with this sample and the VLA FIRST survey image. This object is most likely to be a twin jet FRI source, a claim backed up by comparison of the flux density measurements (see Table 4).

1030+4309: The radio image of 1030+4309 shows extensive emission decreasing in surface brightness away from the core, albeit on fairly small (i.e. arcsecond) scales which explains the fairly steady flux measurements across different arrays. The 8-GHz image reveals the core, the bright peak 2.5 arcseconds to the north and a faint south western extension. The radio morphology points to this source being an FRI quasar although it is possible that the extended emission represents plumes diverted from the hotspots at the ends of short jets.

1032+4932: All evidence suggests that this quasar has a distorted classical double FR II structure associated with it. The flux density remains steady for all array configurations. The 8-GHz radio map shows the four components also visible in the 1.4-GHz image although the southern extension and north eastern component are very weak. The faint extended emission to the east may represent diffuse emission associated with the quasar although the radio emission is very much dominated by the core and the peak nearest to it.

1033+4116: Radio imaging of this object revealed only a hint of an eastern extension at B-array, also seen in the FIRST survey image. The cause of the variation in the flux density values is most probably source variability. The true morphology of this source remains inconclusive.

1037+4650: The 1.4-GHz image shows a prominent south western extension, and also an extension to the north east, suggesting this object is a FRI source. The 8-GHz image reflects this, showing the quasar and faint extensions coincident with the ones visible at 1.4 GHz and no evidence of any hotspots.

1038+3729: Another probable fat double or hybrid source with morphology remarkably similar to that of 1021+4523 showing a pair of jets with a southern hotspot and a more diffuse northern counter jet. The east-west feature seen running between the core and the southern hotspot was coincident with the sidelobe structure of a strong confusing source to the east although, after careful consideration, we think it is unlikely that this feature is an imaging artifact due to its curvature. It is uncertain whether it is associated with the quasar, although radio galaxies have been seen to exhibit unusual X-shaped wing structures (e.g. Dennett-Thorpe et al., 2002). The stronger peak on the eastern edge of the map is coincident with a nearby unrelated source. The jets of this source also appear to be swept back slightly in an easterly direction, possibly a result of motion through the ambient medium.

1040+4449: This object has extended emission similar to that of E1821+643 (Blundell & Rawlings, 2001) and flux density measurements pointing to a FRI classification. The slight bend in the major axis may indicate some motion relative to the surrounding gaseous medium in a north-westerly direction.

1040+4529: It is not possible to draw a definite conclusion as to the nature of this object. The feature to the east of the quasar may be a faint jet and the VLA FIRST survey image hints at an eastern extension, however the flux density values suggest that if there is any diffuse extended emission it is below detectability for the observations presented in this paper.

1054+4541: At a redshift of 2.5 this is the most distant object in the sample. Flux density measurements from different VLA arrays suggest there is extended structure associated with this object and there is a hint of oppositely directed jet activity in the radio image. The extended features in this image are real, but are not coincident with any compact features in a high-resolution MERLIN image (Heywood et al., in prep.).

1057+4556: The final object in the sample is another highly asymmetric FR II classical double. It is in many ways morphologically similar to 1022+3931 and 1032+4932, with large differences in separation between the core and each hotspot and what appears to be a diverted plume associated with one hotspot.

4.2 Radio luminosity and redshift considerations

Figure 6 shows 151-MHz radio luminosity plotted against redshift for the objects in the sample. The horizontal lines show the traditional FRI / FR II break luminosity at 151 MHz assuming spectral indices of 0.5 (dashed) and 1.0 (solid). The curved lines show the detection limits as a function of redshift for a source of flux density 0.1 Jy for assumed spectral indices of 0.5 and 1.0.

By examining this plot it is evident that there exist FRI type sources over a large range in luminosity and above the traditional FRI / FR II break. If 1037+4650 and 1054+4541 (the labelled, filled circles on Figure 6) are indeed bona fide FRI sources then the luminosity range for FRI type quasars extends to over 10^{27} W Hz⁻¹ sr⁻¹ in the cosmology assumed in this paper. Whether these objects are FRI sources is not completely certain however it is noteworthy that they are definitely do not have compact hotspots associated with edge-brightened extremities, as would be characteristic of a classical double source.

There is the possibility that these high redshift objects could resemble, for example, B2 1108+27 (Owen et al., 2000). This source initially appeared to be an arcminute-scale FRI-type structure on the basis of the NVSS image, however a two hour integration with the VLA in D-array revealed that the emission associated with the jets of this object actually extended to an angular size of 30 arcminutes, corresponding to a 1-Mpc structure. It is possible that the radio images of sources such as 1037+4650 and 1054+4541 presented in this paper simply represent the inner regions of sources similar to B2 1108+27. Detection of faint, extended emission around these sources could only be confirmed with subsequent very deep, pointed compact-array observations.

Another consideration is the fact that quasars have bright cores and possibly exhibit very strongly beamed emission. Strongly beamed jets may influence the classification of an object by concentrating the emission into a small angular size. Our initial selection however was not made at a frequency at which Doppler boosting operates (e.g. 1.4 GHz),

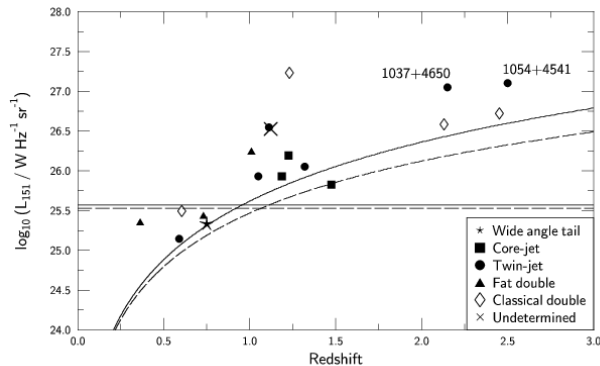


Figure 6. The 151-MHz radio luminosity against redshift. The horizontal lines show the traditional FRI / FR II break luminosity adjusted for a frequency of 151 MHz, and the curved lines show the flux density limit as a function of redshift for a 0.1-Jy source. For both of these indicators the assumed spectral indices are 0.5 and 1.0 for the dashed and solid lines respectively.

but at the lower frequency of 151 MHz which measures on isotropic lobe emission.

If a more cautious approach is adopted and it is assumed that 1037+4650 and 1054+4541 cannot be considered to be FRI sources, there are still FRI-type twin-jet sources with luminosities of up to $10^{26.4}$ $\text{W Hz}^{-1} \text{sr}^{-1}$ (1030+4309), almost a factor of 10 above the traditional FRI / FR II break.

Furthermore, although FRI type sources are observed with luminosities over a factor of ten higher than the traditional FRI / FR II break, there are no FR II objects (with the borderline exception of 1022+3931) with luminosities significantly below the break. For this reason we believe that the FRI / FR II break is still significant as a threshold below which classical doubles are not in general found, although clearly a deeper understanding of FR I evolution is required, building on the existing work on low-luminosity radio sources (e.g. Clewley & Jarvis, 2004).

A second possible explanation for the presence of these high-luminosity FRI quasars arises by considering jet power and the environment surrounding the object. A low power jet will only give rise to an FRI type structure since the flow is subsonic. Shock fronts do not occur when the material collides with the intergalactic medium and therefore no hotspots are ever formed at the jet extremities. It is postulated here that high power jets can however give rise to both FRI and FR II morphologies depending on their environment. For a smooth and rarefied local environment a high power jet can continue relatively unhindered and remain collimated until it strikes the boundary with the IGM, resulting in shock fronts and the increased brightness hotspots which characterise a FR II classical double. For a dense or clumpy local environment the jet may lose much of its momentum and dissipate its energy in a more gradual fashion resulting in an FRI type object.

At higher redshift the environments surrounding active galactic nuclei may well be denser and clumpier than those of the local Universe. Jets associated with high redshift environments would be more prone to disruption than those associated with objects in the local Universe, thus only well

collimated, high power jets would produce FR II type structures (Barthel & Miley, 1988).

5 CONCLUSIONS

The most obvious conclusion that can be drawn from these results is that E1821+643 is not a unique exception as an FRI quasar and that FRI quasars are not uncommon amongst populations selected to be both radio-loud and quasars: objects with broad emission lines can give rise to FRI structures, which apparently have low power radio jets.

The two classes of radio morphology described by Fanaroff & Riley (1974) appear to apply to quasars, in that quasars exist in both FRI and II categories. However, our results also show that there is no sharp transition across a certain luminosity as we observe FRI quasars with luminosities at least a factor of 10 above the traditional FRI / FR II break.

The source 1023+4824 is the only object in the sample to show a *clear* classical double morphology. Three sources which are dominated by core and hotspot emission and could therefore be thought of as hybrid FR II classical double sources exhibit obvious similarities (1022+3931, 1032+4932 and 1057+4556). All three of these feature a double hotspot and are highly asymmetric about the core. Generally the sources are either FRI twin jet (or FRI-like) sources (e.g. 1023+3604, 1030+3346, 1030+4309, 1037+4650, 1040+4449) or unusual hybrid or fat double sources (e.g. 1009+4655, 1021+4523, 1038+3729).

Most objects observed at $z \sim 0.6$ in the 7C quasar survey are FR Is (see Figure 6), and lie below the traditional FRI/FR II break in luminosity. The lack of FRI quasars in the 3C survey may be due, at least in part, to rarity issues. Although the comoving volumes probed by 3CRR and 7C are comparable (3CRR probes $\sim 1 \times 10^8$ Mpc^3 to a redshift of 0.1, 7C probes $\sim 2 \times 10^8$ Mpc^3 to a redshift of 0.6), quasars are more numerous at $z \sim 0.6$ than at $z \sim 0.1$. However, it does seem from studies of complete samples of radio sources at $z \sim 0.6$ (McLure et al., 2004; Mitchell, 2005) that a typical $L_{151} \sim 10^{(25-25.5)}$ $\text{W Hz}^{-1} \text{sr}^{-1}$ radio source at $z \sim 0.6$ has a FRI radio structure but has neither an observed quasar nucleus (as signified by, for example, the presence of broad H α emission lines) nor evidence for any buried nucleus of comparable intrinsic luminosity (inferred, e.g., from strong narrow emission lines).

Again with reference to Figure 6, at $z \sim 1.25$ we seem to generally observe FR I-like structures. In the 7C quasar survey, FR I objects exist at higher radio luminosities ($10^{(26-26.5)}$ $\text{W Hz}^{-1} \text{sr}^{-1}$) than those observed in the 3C survey at low redshift. There is thus evidence that the division between FRI and FR II radio sources changes with z , in the sense that FR Is can exist above the traditional break luminosity at higher redshifts. The obvious explanation for this (which is therefore also likely to affect the $z \sim 0.5$ population) is a systematic change in the environments of radio sources with cosmic epoch (see Section 4.2).

For the objects at $z \sim 2.3$ the data presented here have shown that the furthest extents of these sources are not coincident with hotspots, but it remains open as to whether these objects are truly FR Is or have, for instance, disrupted

or precessing jets. Further high resolution radio imaging would be useful to resolve such questions.

Disproving the idea that *FR I* radio structures cannot be associated with a quasar (i.e. an accreting black hole central engine) is quite an important conclusion. It has recently become clear from surveys with Spitzer (e.g. Martinez-Sansigre et al., 2005) that most quasar activity, and hence black hole growth, in the universe has been missed by optical and X-ray surveys due to obscuration by dust and gas. Many of these obscured quasars have radio luminosities and spectral indices consistent with the hypothesis that they are associated with *FR I*-like radio jets (Martinez-Sansigre et al., 2006). The objects observed in this paper may be unobscured examples of the same phenomenon. The growth of supermassive black holes may thus go hand-in-hand with *FR I*-like jet output which may have critical effects on the evolution of galaxies (e.g. Croton et al., 2005) and larger-scale structures.

ACKNOWLEDGEMENTS

IH and SR thank PPARC and KMB thanks the Royal Society for a University Research Fellowship. We also thank the referee for useful comments. The VLA is a facility of the NRAO operated by Associated Universities, Inc., under cooperative agreement with the National Science Foundation. This research has made use of NASA's Astrophysics Data System.

REFERENCES

- Baars, J. W. M., Genzel, R., Pauliny-Toth, I. I. K., & Witzel, A. 1977, *A&A*, 61, 99
- Barthel, P. D. 1989, *ApJ*, 336, 606
- Barthel, P. D., & Miley, G. K. 1988, *Nat*, 333, 319
- Baum, S. A., Zirbel, E. L., & O'Dea, C. P. 1995, *ApJ*, 451, 88
- Becker, R. H., White, R. L., & Helfand, D. J. 1995, *ApJ*, 450, 559
- Blundell, K. M., 2005, *Phil. Trans. Roy. Soc.*, 363, 645
- Blundell, K. M., & Rawlings, S. 2001, *ApJL*, 562, L5
- Blundell, K. M., Rawlings, S., & Willott, C. J. 1999, *AJ*, 117, 677
- Clewley, L., & Jarvis, M. J. 2004, *MNRAS*, 352, 909
- Condon, J. J., Cotton, W. D., Greisen, E. W., Yin, Q. F., Perley, R. A., Taylor, G. B., & Broderick, J. J. 1998, *AJ*, 115, 1693
- Croton, D. J., et al. 2005, *MNRAS*, 356, 1155
- Dennett-Thorpe, J., Scheuer, P. A. G., Laing, R. A., Bridle, A. H., Pooley, G. G., & Reich, W. 2002, *MNRAS*, 330, 609
- Erlund, M. C., Fabian, A. C., Blundell, K. M., Celotti, A., & Crawford, C. S. 2006, *MNRAS*, 371, 29
- Falcke, H., Gopal-Krishna, & Biermann, P. L. 1995, *A&A*, 298, 395
- Fanaroff, B. L., & Riley, J. M. 1974, *MNRAS*, 167, 31P
- Goldschmidt, P., Kukula, M. J., Miller, L., & Dunlop, J. S. 1999, *ApJ*, 511, 612
- Gopal-Krishna, & Wiita, P. J. 2002, *New Astronomy Review*, 46, 357
- Kaneda, H., et al. 1995, *ApJL*, 453, L13
- Hooper, E. J., Impey, C. D., Foltz, C. B., & Hewett, P. C. 1996, *ApJ*, 473, 746
- Kellermann, K. I., Sramek, R. A., Schmidt, M., Green, R. F., & Shaffer, D. B. 1994, *AJ*, 108, 1163
- Kukula, M. J., Dunlop, J. S., Hughes, D. H., & Rawlings, S. 1998, *MNRAS*, 297, 366

- Martínez-Sansigre, A., Rawlings, S., Lacy, M., Fadda, D., Marleau, F. R., Simpson, C., Willott, C. J., & Jarvis, M. J. 2005, *Nat*, 436, 666
- Martínez-Sansigre, A., Rawlings, S., Garn, T., Green, D. A., Alexander, P., Klöckner, H.-R., & Riley, J. M. 2006, *MNRAS*, 373, L80
- McLure, R. J., Willott, C. J., Jarvis, M. J., Rawlings, S., Hill, G. J., Mitchell, E., Dunlop, J. S., & Wold, M. 2004, *MNRAS*, 351, 347
- Miller, L., Peacock, J. A., & Mead, A. R. G. 1990, *MNRAS*, 244, 207
- Miller, P., Rawlings, S., & Saunders, R. 1993, *MNRAS*, 263, 425
- Mitchell, E. K., 2005, PhD thesis, Univ. Oxford
- Owen, F. N., & Laing, R. A. 1989, *MNRAS*, 238, 357
- Owen, F. N., Ledlow, M. J., Eilek, J. A., Kassim, N. E., Miller, N., Dwarakanath, K. S., & Ivison, R. J. 2002, *The Universe at Low Radio Frequencies*, 199, 171
- Pearson, T. J., Blundell, K. M., Riley, J. M., & Warner, P. J. 1992, *MNRAS*, 259, 13P
- Rawlings, S., & et al. 1998, *ASSL Vol. 226: Observational Cosmology with the New Radio Surveys*, 171
- Riley, J. M., Rawlings, S., McMahon, R. G., Blundell, K. M., Miller, P., Lacy, M., & Waldram, E. M. 1999, *MNRAS*, 307, 293
- White, R. L., et al. 2000, *ApJS*, 126, 133

This paper has been produced using the Royal Astronomical Society/Blackwell Science \LaTeX style file.